

Global Biogeochemical Cycles



RESEARCH ARTICLE

10.1029/2020GB006848

Key Points:

- Direct measurements show that air-water CO₂ exchange over seagrass meadows is of similar magnitude to carbon burial rates
- Key drivers are tides, temperature, light, and wind, which off in importance over hourly seasonal time scales
- Surface drag coefficients were greater than open water prediction, suggesting a near-universal gas transfer enhancement across all sites

Supporting Information:

Supporting Information may be found in the online version of this article.

Correspondence to:

B. Van Dam,
vandam.bryce@gmail.com

Citation:

Van Dam, B., Polsenaere, P., Barreras-Apodaca, A., Lopes, C., Sanchez-Mejia, Z., Tokoro, T., et al. (2021). Global trends in air-water CO₂ exchange over seagrass meadows revealed by atmospheric Eddy Covariance. *Global Biogeochemical Cycles*, 35, e2020GB006848. <https://doi.org/10.1029/2020GB006848>

Received 1 OCT 2020

Accepted 25 MAR 2021

Global Trends in Air-Water CO₂ Exchange Over Seagrass Meadows Revealed by Atmospheric Eddy Covariance

Bryce Van Dam¹ , Pierre Polsenaere² , Aylin Barreras-Apodaca³, Christian Lopes⁴ , Zulia Sanchez-Mejia³ , Tatsuki Tokoro^{5,6}, Tomohiro Kuwae⁶ , Lucia Gutiérrez Loza⁷, Anna Rutgersson⁷ , James Fourqurean⁴, and Helmuth Thomas¹

¹Institute of Carbon Cycles, Helmholtz-Zentrum Hereon, Geesthacht, Germany, ²Ifremer, Laboratoire Environnement et Ressources des Pertuis Charentais (LER-PC), BP133, La Tremblade, France, ³Instituto Tecnológico de Sonora, Ciudad Obregón, México, ⁴Department of Biological Sciences and Center for Coastal Oceans Research, Florida International University, Miami, FL, USA, ⁵Coastal and Estuarine Environment Research Group, Port and Airport Research Institute, Yokosuka, Japan, ⁶National Institute for Environmental Studies, Center for Global Environmental Research (CGER), Office for Atmospheric and Oceanic Monitoring, Tsukuba, Ibaraki, Japan, ⁷Department of Earth Sciences, Uppsala University, Uppsala, Sweden

Abstract Coastal vegetated habitats like seagrass meadows can mitigate anthropogenic carbon emissions by sequestering CO₂ as “blue carbon” (BC). Already, some coastal ecosystems are actively managed to enhance BC storage, with associated BC stocks included in national greenhouse gas inventories. However, the extent to which BC burial fluxes are enhanced or counteracted by other carbon fluxes, especially air-water CO₂ flux (FCO₂) remains poorly understood. In this study, we synthesized all available direct FCO₂ measurements over seagrass meadows made using atmospheric Eddy Covariance, across a globally representative range of ecotypes. Of the four sites with seasonal data coverage, two were net CO₂ sources, with average FCO₂ equivalent to 44%–115% of the global average BC burial rate. At the remaining sites, net CO₂ uptake was 101%–888% of average BC burial. A wavelet coherence analysis demonstrated that FCO₂ was most strongly related to physical factors like temperature, wind, and tides. In particular, tidal forcing was a key driver of global-scale patterns in FCO₂, likely due to a combination of lateral carbon exchange, bottom-driven turbulence, and pore-water pumping. Lastly, sea-surface drag coefficients were always greater than the prediction for the open ocean, supporting a universal enhancement of gas-transfer in shallow coastal waters. Our study points to the need for a more comprehensive approach to BC assessments, considering not only organic carbon storage, but also air-water CO₂ exchange, and its complex biogeochemical and physical drivers.

Plain Language Summary Carbon storage is a valuable ecosystem service of seagrass meadows, serving as a possible pathway to draw down atmospheric carbon dioxide (CO₂) levels. However, this approach may be unsuccessful if carbon storage in sediments is exceeded by the release of CO₂ from the water. To better understand the scope of this problem, we compiled all available measurements of air-water CO₂ exchange over seagrass meadows. We found that rates of CO₂ release or uptake were indeed large, even when compared with potential rates of carbon storage in seagrass soils. However, these large air-water exchanges of CO₂ did not occur for the same reason everywhere. While light availability was sometimes a strong predictor of air-water CO₂ exchange, tidal mixing and temperature were also very important, revealing a much more complex network of drivers than previously thought. Despite these diverse conditions, we found one key similarity across all sites, in that rates of air-water gas transfer appear to always be greater than would be expected for the open ocean. Taken together, the results of our study show that assessments of carbon storage in coastal seagrass ecosystems will be incomplete if they do not consider exchanges of CO₂ between the water and air.

1. Introduction

The coastal ocean plays a disproportionately large role in global and regional carbon (C) cycles (Fennel et al., 2019; Friedlingstein et al., 2019; Laruelle et al., 2018). In particular, seagrass-inhabited regions receive large quantities of terrestrial and marine organic carbon, much of which is sequestered in sediments and stabilized by extensive root mats (Prentice et al., 2020; Röhr et al., 2018). Carbon fixed locally by seagrasses

© 2021. The Authors.

This is an open access article under the terms of the [Creative Commons Attribution License](https://creativecommons.org/licenses/by/4.0/), which permits use, distribution and reproduction in any medium, provided the original work is properly cited.

and their epiphytes is also buried here, constituting a net removal of C from the atmosphere (Duarte et al., 2005; Kennedy et al., 2010). Despite some uncertainty regarding its ultimate source, this “blue carbon” reservoir (Kuwae & Hori, 2019; Macreadie et al., 2019) is a globally significant, yet sensitive, carbon stock (Fourqurean et al., 2012). However, these relatively high C burial rates in seagrass meadows, reaching $0.22 \text{ g C m}^{-2} \text{ yr}^{-1}$ (Duarte et al., 2005), must also be considered in the context of other C flows through the ecosystem, which acts synergistically or antagonistically to increase or decrease net C sequestration.

For example, the biotic or abiotic formation and burial of calcium carbonate in seagrass beds consume alkalinity, thereby generating CO_2 (Burdige et al., 2010; Burdige & Zimmerman, 2002; Hu & Burdige, 2007). Similarly, the degradation of organic matter in anoxic sediments produces CH_4 and N_2O at rates that may affect the net global warming mitigation potential of seagrass meadows (Oreska et al., 2020). As a result, some seagrass beds, especially those receiving large loads of allochthonous organic matter (Al-Haj & Fulweiler, 2020), or those where calcification rates are high (Howard et al., 2018), can be pushed towards net C source status, despite high rates of autotrophic C fixation (Macreadie et al., 2017; Sanders et al., 2019). In particular, the extent to which calcification mitigates photosynthetic CO_2 uptake, pushing seagrass ecosystems towards CO_2 source status remains a hotly debated topic (Howard et al., 2018; Sanders et al., 2019). While some calcium carbonate mineral is imported from adjacent systems and should not enhance CO_2 emissions (Saderne et al., 2019), confirmation of the role of calcification on air-water CO_2 exchange over seagrass meadows is still lacking (Macreadie et al., 2019).

Seagrass meadows may also vary between net ecosystem heterotrophy and autotrophy over daily to weekly time scales (Berg et al., 2019; Gazeau et al., 2005; Van Dam, Lopes, et al., 2019). Elsewhere, the anaerobic generation of alkalinity, largely through sulfate reduction and burial (Dollar et al., 1991) and denitrification (Eyre & Ferguson, 2002), can increase the buffering capacity of the overlying water, enhancing atmospheric CO_2 uptake. Advection can also play a significant role, as seagrasses in river-dominated estuaries may receive waters over-saturated in CO_2 , which is subsequently degassed in the wind-exposed coastal zone (Röhr et al., 2018). Regardless of the mechanism, it is clear that C sequestration in “blue carbon” ecosystems is not simply the product of long-term organic carbon burial in sediments. Many other processes consume or produce dissolved inorganic carbon (DIC), such as calcification and anaerobic metabolism, respectively, thereby affecting air-water CO_2 fluxes (FCO_2), pushing these ecosystems towards net carbon sink or net source, independent of the organic carbon burial flux.

Given the broad global distribution of seagrasses, and the various coastal typologies they inhabit, it is no surprise that net ecosystem metabolism exhibits substantial geographic trends (Duarte et al., 2010). Similarly, FCO_2 in these systems is not uniform. In some regions, for example, light limitation of photosynthesis may play a critical role in net ecosystem productivity (Berg et al., 2019; Long et al., 2015) and CO_2 uptake (Gazeau et al., 2005; Tokoro et al., 2014). Elsewhere, due to greater turbidity or water depth, this factor may carry little leverage, exceeded in importance by tides (Polensaere et al., 2012) or water temperature (Van Dam, Lopes, et al., 2020). Where temperature and biology allow, net ecosystem calcification may instead dominate water column carbonate chemistry (Perez et al., 2018; Van Dam, Lopes, et al., 2019). These reasons and others may contribute to differences in FCO_2 for seagrass meadows located at comparable latitudes or in similar climates.

Rates of carbon burial can be reliably assessed using natural and anthropogenic radioactive tracers, integrating this process over a sufficiently long period to accurately characterize burial over decadal to centennial scales. This is in stark contrast to FCO_2 , where extreme temporal variability complicates attempts to integrate this flux over time. Existing “bulk transfer” approaches to quantifying FCO_2 rely on discrete measurements of CO_2 partial pressure ($p\text{CO}_2$), which often miss out on high-frequency variability. These $p\text{CO}_2$ measurements are then combined with a gas transfer coefficient, the parameterization of which is notoriously challenging due to the diverse physical forcing of air-water gas exchange in shallow coastal waters (Borges et al., 2004). For these reasons, direct measurements of FCO_2 are desirable, relative to parameterized estimates. Atmospheric Eddy Covariance (EC) has been used for decades to measure turbulent exchanges of gas and energy over terrestrial ecosystems (Aubinet et al., 2000), and the open ocean (Wanninkhof et al., 2009). While the arrival of under-water EC methods (Berg et al., 2003) has revolutionized studies of benthic oxygen metabolism (Attard et al., 2019), the lack of rapidly responding $p\text{CO}_2$ sensors means that this approach can only indirectly assess air-water CO_2 exchange (Berg et al., 2019). Atmospheric EC

methods have been available for decades, but have only recently begun to be used at nearshore intertidal or subtidal habitats (Chien et al., 2018; Honkanen et al., 2018; Ikawa & Oechel, 2015; Rey-Sánchez et al., 2017) including seagrass meadows (Polsenaere et al., 2012; Tokoro et al., 2014; Van Dam, Lopes, et al., 2020). Advantages of direct EC measurements of FCO_2 include: (1) continuous temporal coverage, (2) existence of standard methods for data processing, and (3) non-invasive and spatially representative measurements.

While direct FCO_2 measurements over seagrass meadows have existed for roughly a decade (Polsenaere et al., 2012), and some regional synthetic efforts have been made (Tokoro et al., 2014), these individual datasets have yet to be synthesized globally. Therefore, a set of very basic questions remains unanswered. Are there global patterns explaining why some seagrass meadows are CO_2 sinks and others are sources? Are these reasons typological, climatological, or simply latitudinal in nature? Are there any generalizable features of air-water CO_2 exchange across these diverse coastal habitats? These questions are central to “blue carbon” science (Legge et al., 2020; Macreadie et al., 2019), but have yet to be addressed. In the present study, we synthesize a data set of direct EC measurements of air-sea FCO_2 over seagrasses. While this data set is limited to only sites in the Northern hemisphere, it is the most complete synthesis to date, representing a broad range in latitude and ecosystem characteristics. We describe global trends in FCO_2 , discuss temporal and spatial variability and associated controls, and compare FCO_2 with literature estimates of carbon burial. A spectral decomposition is also used to identify sets of physical drivers important across temporal scales.

2. Materials and Methods

2.1. Study Sites

Direct EC measurements of FCO_2 were acquired for six subtidal or intertidal sites across a range in seagrass coverage. Together, these sites represent a broad zonal (110°W to 145°E) and latitudinal (24°N to 57°N) range (Figure 1) and are described in Table 1, along with the nearest recorded coastal typology from Dürr et al. (2011). From here on, we will use the acronyms (OES, AR, FK, FU, EES, BA) shown in Table 1, rather than the full names to refer to each site.

2.2. EC Measurements

While different analytical instruments were used at each site (Table 1), all EC measurements were conducted using coincident and rapid (10–20 Hz) measurements of CO_2 concentration and 3-dimensional wind velocity. All EC systems relied on infrared gas analyzers (IRGA) produced by LI-COR Biosciences, USA. These IRGAs were either of open- or closed-path configurations, depending on the environmental and power conditions at each site. Further information regarding the specific EC configurations used at each site can be found in the references shown in Table 1.

2.3. Data Quality Control

For all datasets processed using EddyPro software (Licor Biosciences, USA), data were screened to remove records with quality control (QC) code (Burba, 2010) greater than 1, resulting in a removal of 11.6% of the full data set. A detailed description of this QC criteria is provided elsewhere (Mauder & Foken, 2004), but briefly it seeks to combine tests for steady state and turbulence development into a single QC flag, where values >1 can be considered of “poor quality.” Next, in an effort to screen out data where a terrestrial influence was likely, we removed results where the shear conditions indicated a non-marine flux footprint. As described later, we discarded FCO_2 results when the ratio of u_* / U_{mean} exceeded a threshold of 0.139, which was set as 150% of the average u_* / U_z (0.0924). This step resulted in the removal of an additional 14.6% of the data following QC code screening. Lastly, FCO_2 values greater than 3 standard deviations from the mean ($\text{FCO}_2 > 10.4 \mu\text{mol m}^{-2} \text{s}^{-1}$) were considered anomalous and were removed, representing a final 1.3% of the remaining data set. Cumulatively, these screening steps removed 25.5% of the initial, post-processed data set. In keeping with convention, negative FCO_2 indicates a net CO_2 uptake, while positive values represent CO_2 emission.

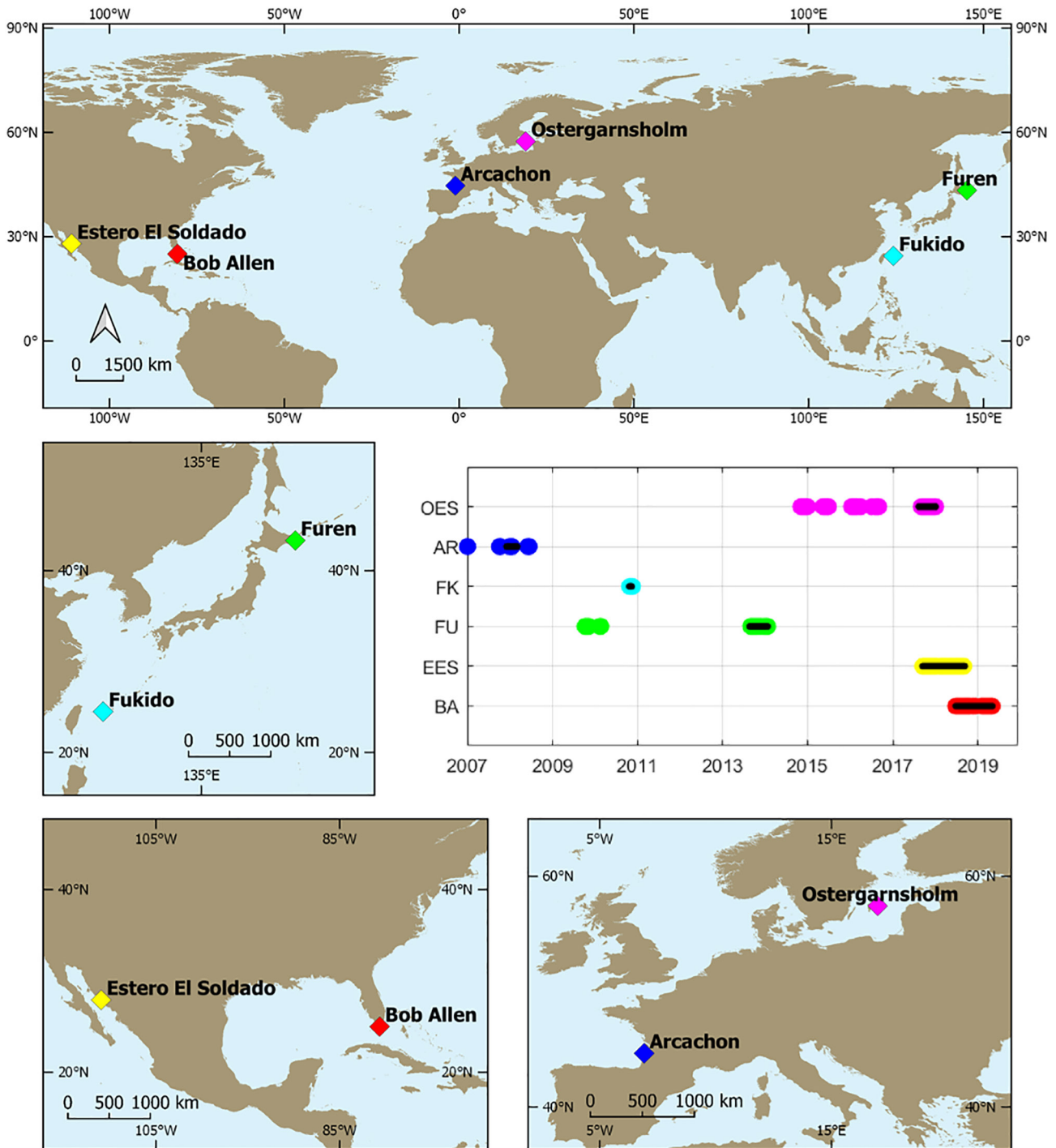


Figure 1. Site Maps, including inset figure of data coverage for each site, where the black bars indicate the subset of reasonably “continuous” data used for the wavelet coherence analysis.

2.4. Energy Balance

Energy balance assessments are important components of terrestrial EC studies, as these energy flows (radiative as well as latent and sensible heat exchanges) directly control local water budgets and hence many ecosystem processes. In an idealized system, inputs of energy net solar radiation (R_n) are exactly balanced by latent (i.e., evaporative) and sensible heat fluxes, LE and H , respectively. Any departure from the 1:1

Table 1

Summary Table Describing Each Site Considered in This Study, Including the Estuarine Typology (Dürr et al., 2011), and Seagrass Community and Coverage Statistics When Available

Site name		Estuarine typology	Seagrass community	Mean daily tidal range (tidal category)	Seagrass biomass (gC or gDW m ⁻²)	Lat-long (decimal degree)	Days of data available (# measurement periods)	Methods reference
Bob Allen Keys, USA	BA	Type VI (Karst)	<i>Thalassia testudinum</i>	0.048 m (small-tidal)	4.8 gC m ⁻²	25.03–80.68	314 (1)	Van Dam, Lopes, et al. (2020)
Estero El Soldado, Mexico	EES	Type VII (Arheic)	<i>Zostera marina</i>	0.40 m (large-tidal•)	-	27.95–110.97	357 (1)	Benítez-Valenzuela & Sanchez-Mejia, (2020)
Furen lagoon, Japan	FU	Type I (Small Deltas)	<i>Zostera marina</i>	0.87 m (large-tidal)	16–318 g DW m ⁻²	43.33 145.26	146 (3)	Tokoro et al. (2014)
Fukido estuary, Japan	FK	Type I (Small Deltas)	<i>Cymodocea serrulata</i> , <i>Thalassia Hemprichii</i> , <i>Enhalus acoroides</i>	0.93 m (large-tidal)	32–88 gDW m ⁻²	24.49 124.23	25 (1)	Tokoro et al. (2014)
Arcachon Bay, France	AR	Type II (Tidal Systems)	<i>Zostera noltii</i>	1.8 m (large-tidal)	93.4–114.9 gDW m ⁻²	44.67–1.67	530 (2)	Polsenaere et al. (2012)
Östergarnsholm, Sweden	OES	-	*Un-determined	<0.5 (small-tidal)	-	57.45 18.98	1,156 (1)	Rutgersson et al. (2020)

Community and cover statistics are from Plus et al. (2010) and Carmen et al. (2019) for AR, from Tokoro et al. (2014) for FU and FK, from Armitage et al. (2011) for BA. Tidal ranges shown here were calculated from mean daily statistics over the entire study period, except for OES, where we apply a literature value of 0.5 m (Sahlée et al., 2008). EES is considered a “large-tidal” site because it is located inside a tidal inlet where appreciable tidal currents exist despite a relatively low tidal range. *Seagrass coverage at OES has not been quantitatively assessed, but historical analysis suggests a mixed community dominated by *Zostera marina* is present throughout these coastal waters (Boström et al., 2003; HELCOM, 2009).

Abbreviations: AR, Arcachon Bay; BA, Bob Allen Keys; EES, Estero El Soldado; FK, Fukido estuary; FU, Furen lagoon; OES, Östergarnsholm.

relationship between R_n and total heat loss ($H + LE$), suggests that EC measurements are missing some energy flux. This could be due to non-stationary conditions, when spatial gradients in a variable (i.e., temperature) are advected past the measurement site, causing, for example, $LE + H$ to be greater/less than R_n . While these measurements may well be “real”, they can also be problematic because they indicate that factors outside the flux footprint have influenced the measured vertical fluxes at a given time. Similarly, energy can be stored in (or lost from) standing water when its temperature changes. In the present study, we have quantified this water-column heat storage (J) as a function of the change in water temperature considering the water depth, specific heat, and density of the water (Van Dam et al., 2020). Because of the very high heat capacity of water, frequent departures from the 1:1 relationship between $H + LE + J$ and R_n can be taken as indicators of lateral water exchange. This is of course concerning for EC studies of FCO_2 in shallow waters, where our goal is to attribute measured FCO_2 to processes happening inside the flux footprint (i.e., the seagrass meadow).

At sites where measurements of water temperature, water height, net solar radiation (R_n ; $W m^{-2}$), latent heat flux (LE ; $W m^{-2}$), and sensible heat flux (H ; $W m^{-2}$) were available, it was possible to construct an approximate energy budget. We determine the closure of this energy balance as the difference between R_n and the sum of LE , H , and J , integrated over 24 h (BA, EES, FK, OES) or 6 h when water-side measurements were limited (AR). When R_n data were absent, R_n was estimated from photosynthetically active radiation (PAR; $\mu mol photons m^{-2} s^{-1}$) using an empirical relationship ($R_n = -0.60 * PAR - 0.12$; linear $R^2 = 0.98$) constructed using the combined data set from this study.

The energy balance at OES is somewhat more challenging to assess, in part because of a relatively complex bathymetry, which makes it difficult to estimate the water depth over which the water-column energy storage (J) should be integrated. The presence of seasonal and periodic stratification, as well as greater absolute water depths (up to 40 m), further complicates the energy balance here (Rutgersson et al., 2020). Therefore,

for OES, we calculated J using a water depth of 5 m, which was the depth at which water temperature was measured.

2.5. Time-Frequency Analysis

A wavelet coherence analysis (Grinsted et al., 2004; Torrence & Compo, 1998) was carried out to analyze the dependence of FCO_2 on net solar radiation (R_n), water depth (Z_{water}), air temperature (T_{air}), water temperature (T_{water}), wind speed (U_{mean}), and wind direction (U_{dir}) across temporal scales and through time. This analysis was completed in the “wavelet-coherence” package for MATLAB R2017 (Grinsted et al., 2004). Due to the sporadic nature of these coastal EC deployments, the temporal coverage is somewhat patchy, creating a problem for time-series analysis. So, prior to wavelet coherence analysis, the largest period of contiguous data availability was identified for each site (black bars shown in Figure 1), and only this period was used for subsequent wavelet analysis. This choice improved data quality at hourly to monthly time scales, but necessarily involved a loss of information at longer scales. The small remaining gaps in the pseudo-continuous datasets (due to poor QC, instrument failure, etc) were filled with mean statistics for each variable, and the edges were padded with zeros (Grinsted et al., 2004). Because this wavelet analysis requires that the probability distribution function is approximately normal, we used the “normalizepdf” function to transform each data set to have a mean of zero and a unit variance (Grinsted et al., 2004). We finally applied a Morlet wavelet to the time series using the “wtc” function (Grinsted et al., 2004) and estimated the 95% confidence intervals with 15 Monte Carlo simulations.

3. Results and Discussion

3.1. Energy Balance

The energy balance closure was best for BA, with daily average R_n closely balanced by net heat losses ($H + LE + J$) (Figures 2a and S1). This was not the case for the remaining sites for which a complete energy balance could be assessed (EES, FK, FU, AR, OES). At EES, most daily average heat losses ($H + LE + J$) fell below the 1:1 line (Figures 2b and S1), indicating either a measurement error, or the presence of a missing heat flux that we currently do not account for. At EES, this missing heat flux could plausibly be related to horizontal advection and tidal exchange with the adjacent upwelling system. Similarly, low heat losses relative to R_n were observed at OES (Figure 3b), but the microtidal nature of this site suggests that the energy budget imbalance here could be related to horizontal advection and wind-driven upwelling. The energy balance is further complicated at OES due to periodic stratification and variable water depths, and our approach of assuming a single, average water height to calculate J , may not be appropriate.

At FU, $H + LE + J$ was always much less than R_n , indicating that water column heating was a major, yet unaccounted for, energy sink. In contrast to the previous sites where $H + LE + J$ was typically less than R_n (EES, OES, FU), daily heat losses were always greater than R_n at both AR and FK (Figures 2c, 3a, and S1). This suggests the presence of an additional heat source, beyond net solar radiation (R_n). Since tidal ranges are relatively large at both AR and FK, we suggest that tidal mixing was the source of warmer water (following solar heating of exposed tidal flats), allowing heat losses through H and LE to exceed net solar inputs.

To further illustrate the role of tidal forcing on energy budgets, we calculate an energy balance residual (EBR) as ($\text{EBR} = [J + H + LE] - R_n$), which represents the departure from the 1:1 line in Figure S1. When EBR is plotted against the range in water height, it becomes clear that tidal forcing plays a key role in governing energy balances across a global distribution of seagrass meadows (Figures 2 and 3). At both microtidal (BA) and tidal (EES and FK) sites, the intercept of EBR with tidal range is not significantly different from zero ($\alpha = 0.05$), indicating that the energy budget is in approximate closure when tidal forcing is not present. The y -intercept was not zero at FU ($-374.7 \pm 243.9 \text{ W m}^{-2}$), but the presence of a significant negative relationship between EBR and tidal range supports the role of tidal exchange as a sink for heat.

At BA, there appears to be little energy “leakage” due to tidal advection, as EBR does not vary with the daily range in water height (Figure 2a). However, at both tidal sites (EES and FK), there is a significant linear correlation between EBR and the tidal range ($\alpha = 0.05$). This relationship is positive for FK, such that energy inputs from R_n are exceeded by loss through LE , H , or J , with the difference increasing with tidal range

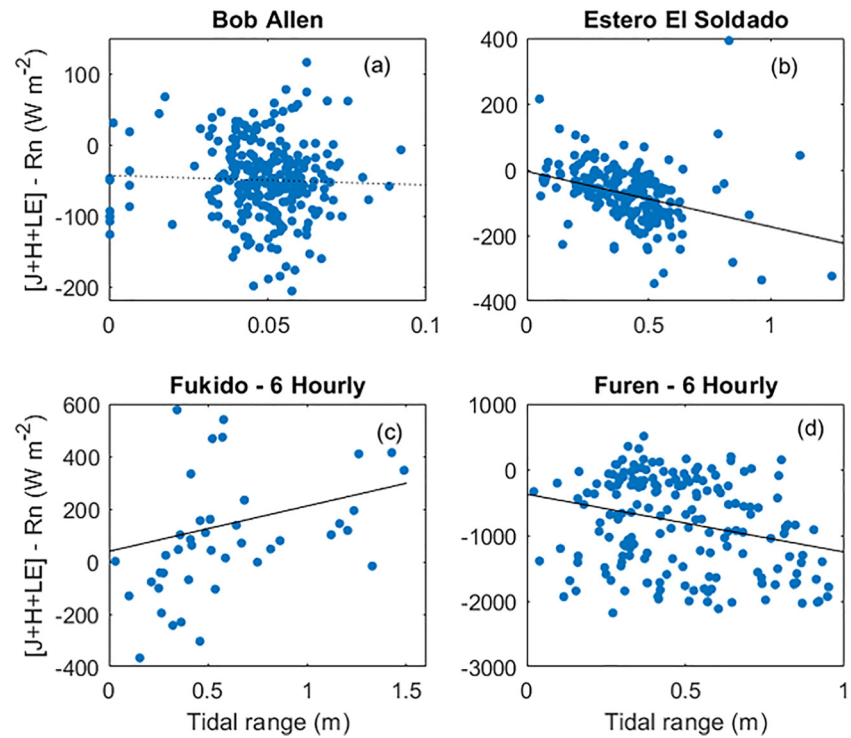


Figure 2. Energy balance residual EBR (difference between $J+H+LE$ and R_n) versus tidal range for BA (a), EES (b), FK (c), and FU (d). Linear slopes for EES, FK, and FU are significantly different from zero and are shown in bold line, while the slope is insignificant for BA (a). EBR, energy balance residual; EES, Estero El Soldado; FK, Fukido estuary; FU, Furen lagoon.

(Figure 2c). This positive EBR implies an input of relatively warm water to the FK embayment, a likely event for a subtropical site during the summer (data for FK are from 23 July to 17 August 2011). The trend is reversed at EES, with EBR becoming more negative with increasing daily tidal range, implying a “leakage” of energy via tidal exchange (Figure 2b). Because the seagrass meadows at EES are influenced by seasonal upwelling in the eastern Gulf of California (Lluch-Cota, 2000), such a heat exchange between warm coastal waters and cooler, recently upwelled water appears plausible.

We used direct, EC measurements of heat fluxes as a conservative tracer, and showed that tidal forcing can explain large-scale trends in energy balances, despite some key site-specific differences. Because the subset of three sites considered here (BA, EES, FK) are at approximately the same latitude (Table 1), the impact of latitudinal differences in LE (Figure 6d) can be excluded as a secondary factor. In subsequent sections, we

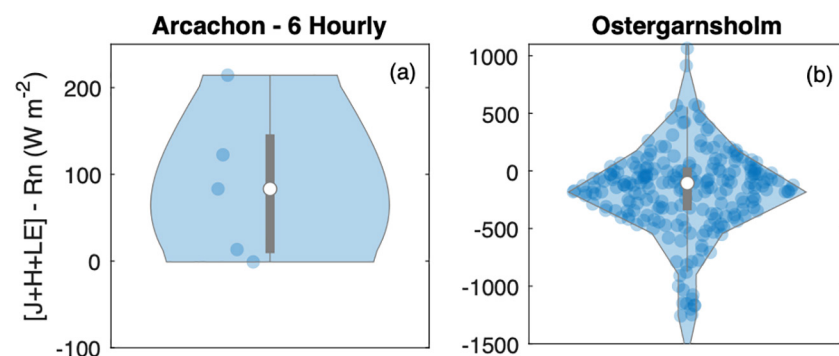


Figure 3. Violin plots of EBR for AR (a) and OES (b). AR, Arcachon Bay; EBR, energy balance residual; OES, Östergarnsholm.

will extend the results of this analysis to a non-conservative constituent, CO₂. We will discuss the impact of tidal mixing on air-water CO₂ exchange, in the context of the coastal “blue carbon” sink.

3.2. General Patterns and Trends in FCO₂

FCO₂ was highly variable at all sites, fluctuating in time between sink (negative FCO₂) and source (positive) behavior. Averaged over the entire study period, however, FCO₂ was negative for four sites (EES, FU, FK, AR) and positive for the other two sites (BA, OES). The spread of FCO₂ in micro-tidal regions (OES, BA) was much more narrow range than in tidal areas (FU, FK, AR, EES), suggesting that the general relationship between tidal forcing and energy fluxes (Figure 2) also applies to air-water CO₂ exchange.

These average CO₂ evasion/invasion rates are plotted (Figure 4) alongside organic carbon burial rates (CBR) taken from a global literature review (Samper-Villarreal et al., 2018 [A], Prentice et al., 2020 [B], Duarte et al., 2005 [C], Kennedy et al., 2010 [D], and Sanders et al., 2019 [E]). Converted into the same unit as FCO₂, these literature CBRs ranged from -0.025 to $-0.23 \mu\text{mol C m}^{-2} \text{s}^{-1}$, for a global average of $-0.126 \pm 0.082 \mu\text{mol C m}^{-2} \text{s}^{-1}$. The comparison of CBR with FCO₂ should be made with some caution, as CBR represents time scales much longer (decades to centuries) compared with our FCO₂ measurements, for which the longest available data set is just over three years long.

Nevertheless, for the sites with complete seasonal coverage (BA, EES, FU, OES), it is apt to make a comparison between the rate of carbon storage in sediments and the exchange of CO₂ with the atmosphere. As is evident in Figure 4, mean FCO₂ was of similar magnitude to CBR (not always the same direction), indicating that both of these biogeochemical fluxes are relevant to the carbon budget of seagrass meadows. Considering an average CBR of $0.126 \mu\text{mol m}^{-2} \text{s}^{-1}$, net emissions at BA released CO₂ to the atmosphere at a rate comparable to 125% of mean global organic carbon burial ($100\% * 0.158/0.126 = 125\%$). Assuming lateral import and export of DIC and alkalinity were balanced, which is plausible at this site (Van Dam, Lopes, Polsenaere, et al., 2020), the net effect of this CO₂ emission was to transition the site from a sink for carbon into a small source. It is likely that the relatively high calcification rates in Florida Bay (Howard et al., 2018) are responsible for generating CO₂ in excess of photosynthetic uptake, pushing this site towards net CO₂ emissions. This is a noteworthy finding in light of the commonly held view that carbonate-rich seagrass meadows can still be CO₂ sinks due to the import of allochthonous CaCO₃ (Saderne et al., 2019). The lack of strong tidal forcing and lateral water exchange at BA adds confidence to our finding of net CO₂ emissions at this site and supports our interpretation that calcification in seagrass meadows can be sufficient to offset autotrophic CO₂ uptake.

Similarly, net CO₂ emissions at OES were 44% of the average global CBR. It should be noted that the greater water depth at OES means that water-column processes are likely more important than benthic processes here in comparison with the other sites. The role of seagrass is therefore relatively more uncertain at this site. At the remaining sites, net negative FCO₂ uptake increased carbon uptake by 888% (FU) and 101% (EES), relative to global average CBR. As discussed later, net CO₂ uptake at these “large-tidal” sites do not necessarily point to increase carbon storage, but rather export of DIC or import of alkalinity to/from adjacent waters. This simple assessment indicates that the consideration of only CBR or FCO₂ alone will bias the magnitude, or even sign (in the case of BA) of the coastal carbon sink. Therefore, we point to a clear need for site-specific measurements of both annually integrated FCO₂ (by EC, for example) and CBR, which together may significantly increase the reliability of coastal carbon accounting.

Differences were also evident in the temporal trends in FCO₂ (Figure 5). Some sites exhibited a clear diel cycle of CO₂ uptake (EES, FK, AR) or release (FU) during the day, while other sites were relatively consistent CO₂ sources (BA, OES). A significant global trend of decreasing latent heat flux (LE) with increasing latitude is evident (Figure 6d), which is expected given the similar global trend of decreasing insolation at higher latitude. On the contrary, no relationship was observed between FCO₂ and latitude (Figure 6b). Instead, as suggested by the variation in FCO₂ with tidal setting (Figure 4), and the poor energy balance closure for large-tidal sites (Figure 2), the best predictor for site-averaged FCO₂ was in fact tidal range (Figure 6a).

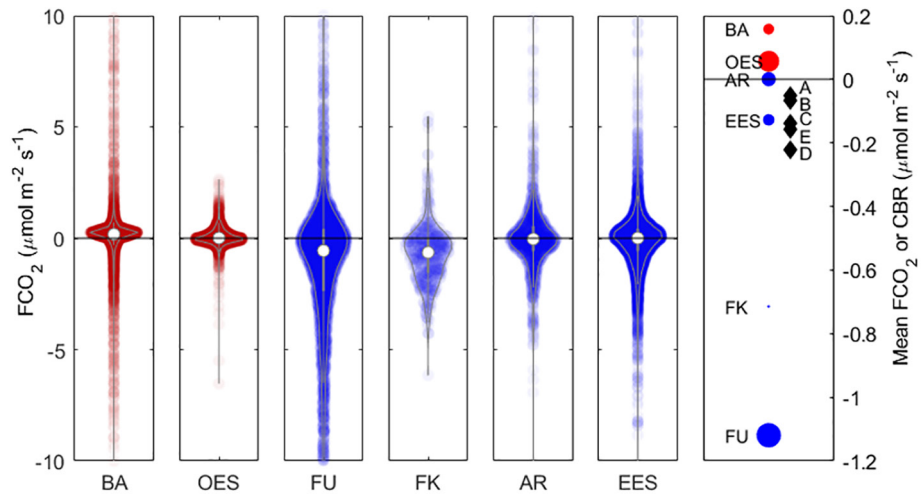


Figure 4. Violin plots of FCO_2 for large-tidal (blue) and small-tidal (red) sites. In the right plot, literature values of carbon burial rates (CBR; black diamonds) are shown alongside average FCO_2 values (blue and red circles), on the same y-axis. The circles are scaled by the number of measurements available for each site. CBR averages are from Samper-Villarreal et al. (2018) (a), Prentice et al. (2020) (b), Duarte et al. (2005) (c), Kennedy et al. (2010) (d), and Sanders et al. (2019) (e). CBR, carbon burial rates.

3.3. Environmental FCO_2 Drivers: Wavelet Coherence

Results from the wavelet coherence analysis are shown in Figure S2, for the following selection of variables: net solar radiation (R_n), water depth (Z_{water}), air temperature (T_{air}), water temperature (T_{water}), wind speed (U_{mean}), and wind direction (U_{dir}). The color indicates the strength of the correlation between each variable and FCO_2 with the phase of this relationship shown by the direction of the arrow. When the variables are in phase (positively correlated), the arrow points right, out of phase (negative correlation) the arrow points left, and when the driver leads FCO_2 by 90° the arrow points down. Subsequently, these results are summarized in Figure 7, which presents the average R^2 for the entire period of record, collapsed along the x-axis in Figure S2. To prevent times of anti-phase correlation from canceling out in-phase correlations (at the same period), the average presented in Figure 7 was calculated using the absolute value of R^2 . As such, Figure 7 only represents the average strength, not the direction, of the correlation between each variable and FCO_2 .

3.3.1. Weekly-Monthly Periods

The importance of each environmental driver on FCO_2 varied across sites and time scales. However, at BA and OES there was generally less power at the daily time scale than there was at weekly-monthly periods. First, as expected for a small-tidal site, Z_{water} was the least predictive variable in the wavelet coherence

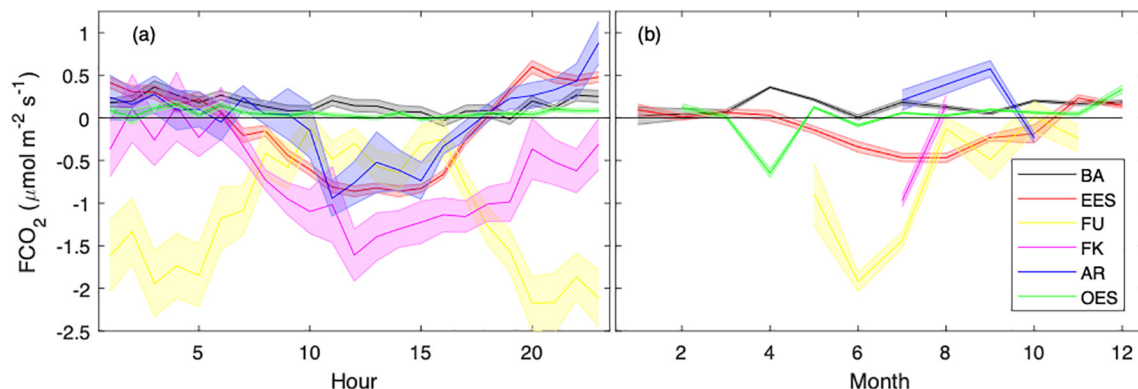


Figure 5. Daily (a) and seasonal (b) climatology of mean FCO_2 for all sites. Negative values of FCO_2 indicate a net CO_2 uptake, while positive values show emission. The shaded areas represent the SE of mean FCO_2 at each hour.

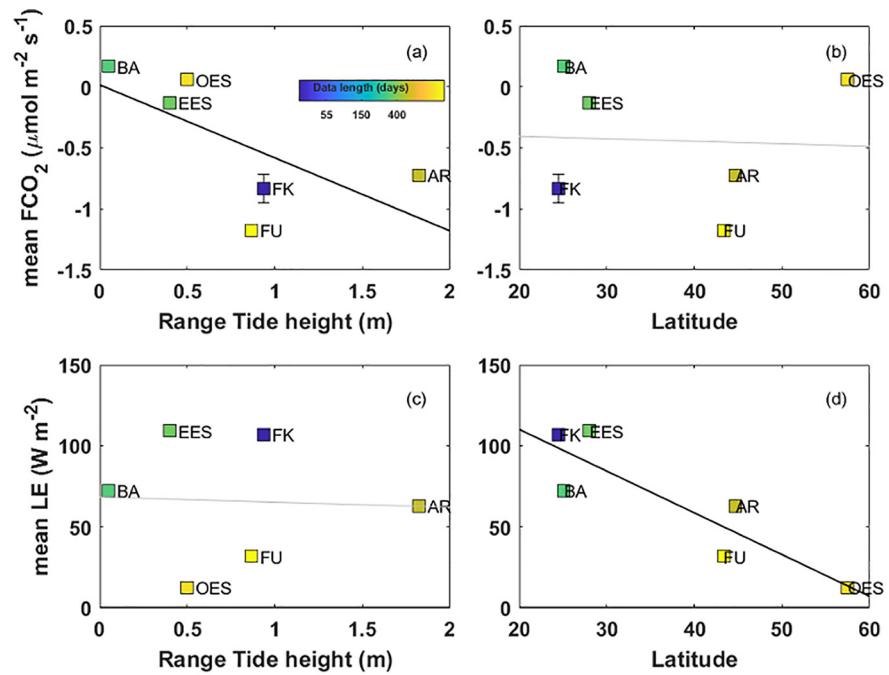


Figure 6. Scatterplots of mean FCO_2 (top panels) and LE (bottom panels) against tidal range and latitude, where the points are colored by the size of the data set. Linear correlations are shown in bold where slopes are significantly different from zero (a and d; $R^2 = 0.504$ and 0.78 respectively, $p < 0.01$). An estimated mean tidal range at OES of 0.5 m (Sahlée et al., 2008) was used for this figure. OES, Östergarnsholm.

analysis at BA, even at the semidiurnal lunar tide (M2 period, ~ 12.5 h). This is in line with the results of the energy budget analysis (Figure 2), supporting the concept that tidal forcing was not an important driver of FCO_2 here. Instead, weekly-monthly scale variations in T_{water} , T_{air} , U_{mean} , U_{dir} were especially prominent as drivers of FCO_2 , rivaling the impact of diel R_n variability (Figures 7a and S2). In particular, the strong positive correlation between T_{water} and FCO_2 across multiple time scales supports (1) the role of ecosystem calcification as a putative CO_2 source, and (2) the importance of thermal forcing of air-water gas transfer (Van Dam et al., 2020).

As was the case for BA, power at the M2 period was not elevated at OES, indicating that tidal forcing was not an important driver of FCO_2 here. Instead, power was focused at longer weekly-monthly time scales at OES (and BA). Because much of the variability at these longer periods is due to synoptic- or meso-scale events, it seems likely that weather patterns at these intermediate time scales may be important drivers of FCO_2 at both OES and BA. Such weather events have also been shown to enhance methane emissions at OES (Gutiérrez-Loza et al., 2019). Fluxes at OES are also known to exhibit a strong seasonal cycle (Rutgersson et al., 2020), although the presence of data gaps prevented the incorporation of seasonality into this wavelet coherence analysis. The relatively deep water at this site may also support the dominance of long time-scales at OES.

3.3.2. Daily and M2 Periods

At both EES and FU, we observed clear bands of power at the daily and M2 time scales (Figure S2), supporting the diel trends present in the FCO_2 climatology (Figure 5). At EES, all variables considered were correlated with FCO_2 at the daily time scale, but traded off in importance over the period of record (Figure S2). For example, U_{mean} was strongly out of phase with FCO_2 during the first half of the study period at EES, while Z_{water} and T_{water} were only weakly correlated with FCO_2 . During the second half of the period of record, this trend reversed, with Z_{water} and T_{water} exceeding U_{mean} as drivers of diel variability in FCO_2 . Seasonal changes in seagrass productivity at EES are a candidate explanation for these corresponding seasonal trends in the drivers of diel-scale variability in FCO_2 and are discussed in detail elsewhere. However, we cannot

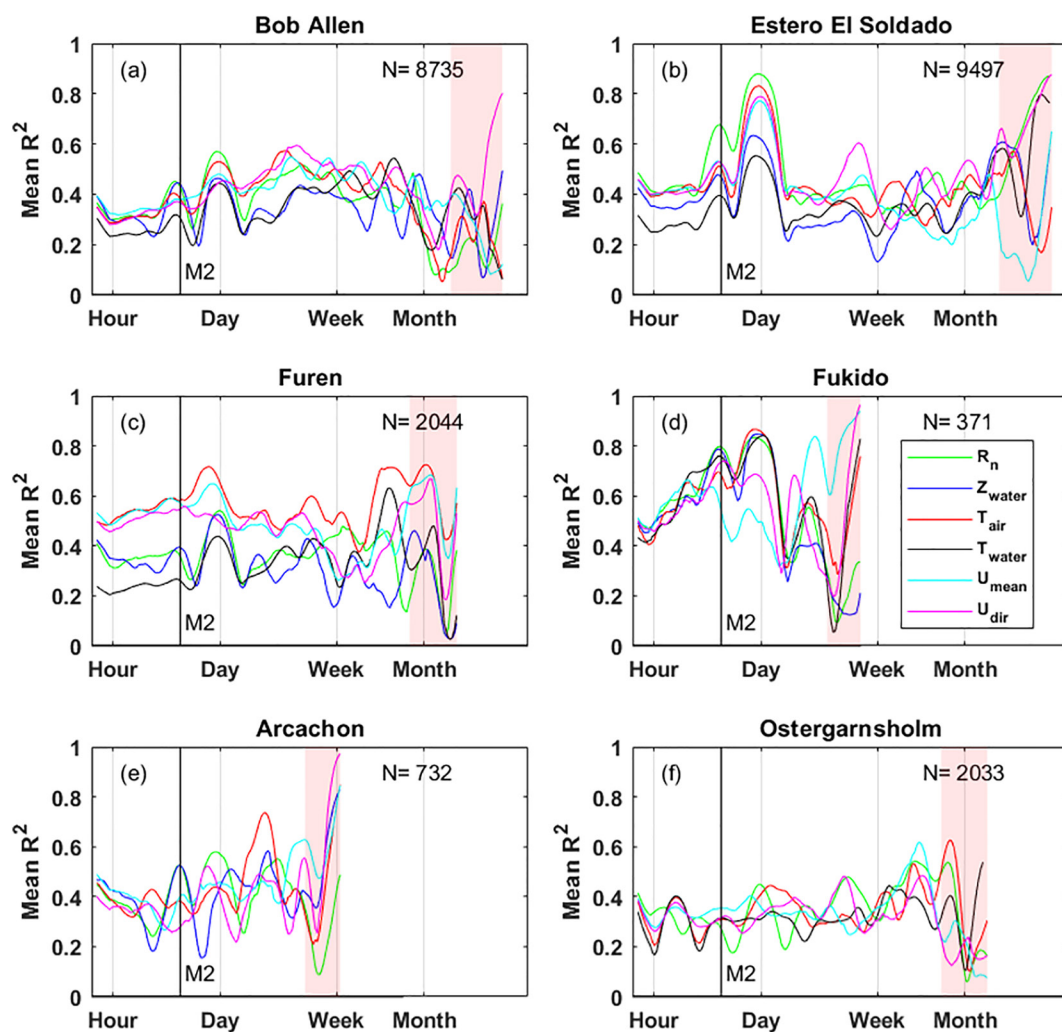


Figure 7. Wavelet coherence analysis summary showing the mean power (R^2) for the relationship between FCO_2 and net solar radiation (R_n), water depth (Z_{water}), air temperature (T_{air}), water temperature (T_{water}), wind speed (U_{mean}), and wind direction (U_{dir}), averaged over the length of each data set (x -axis in Figure S2). The red shading indicates periods where we suspect uncertainty due to edge effects, estimated as 90% of the maximum period. Because positive and negative R^2 values cancel out when averaged, we calculated this statistic using absolute value R^2 . This action effectively sacrifices knowledge of the correlation phase in exchange for a more intuitive summary of the correlation power.

rule out the importance of seasonal upwelling in the eastern Gulf of California (Lluch-Cota, 2000), which may introduce cooler, high- pCO_2 coastal waters to the EES system.

At FU, the diel trend in FCO_2 was opposite of the trend elsewhere, such that CO_2 uptake was greater at night, and decreased during the day (Figure 5). This may appear counterintuitive, given the expectation of greater CO_2 uptake during the day, as supported by photosynthesis-irradiance curves at this site during the summer (Tokoro et al., 2014). However, these estimates of net ecosystem productivity varied from positive to negative over all light regimes in both summer and winter months (Tokoro et al., 2014), indicating that inorganic carbon fluxes were affected by factors other than net ecosystem primary productivity during this time period. Across all periods, T_{air} was the strongest predictor of FCO_2 at the boreal FU site (Figure S2), such that covariations in T_{air} and FCO_2 are in phase (Figure 7c). This in-phase correlation between FCO_2 and T_{air} (and T_{water}) at FU suggests the thermal impact of changing water temperature on pCO_2 , where pCO_2 rises during the day as water warms and decreases overnight as solubility increases (Takahashi et al., 2002), in line with prior findings at Bob Allen Keys, Florida (Van Dam et al., 2020). As with the other large-tidal

sites, correlations between Z_{water} and FCO_2 at FU were strongest at the diel and M2 periods, further supporting the role of tidal forcing on air-water CO_2 exchange.

3.3.3. Wavelet Coherence: Sites With Limited Data

Due to the limited length of data for both FK and AR, it was not possible to assess variability at time scales of a week or more. Nevertheless, tidal forcing appeared to play a prominent role at AR, where Z_{water} and FCO_2 were correlated (generally in-phase) at the diel and M2 periods (Figure S2). This is in line with previous findings demonstrating a general trend of CO_2 uptake during low tide and release during high tide at AR (Polsenaere et al., 2012).

At FK, strong anti-phase correlations were found at the diel time scale for R_n , T_{water} , and T_{air} , while an in-phase relationship was present between FCO_2 and Z_{water} (Figure S2). The presence of anti-phase relationships between FCO_2 and R_n , T_{water} , and T_{air} , strongly suggest photosynthetic CO_2 uptake as a driver of FCO_2 during the short period for which measurements are available at FK. Since CO_2 solubility decreases with increasing temperature, one would expect FCO_2 and air or water temperatures to be in phase. The existing anti-phase relationship between these variables suggests that something other than thermal forcing, namely biological CO_2 fixation, caused the daytime CO_2 uptake at FK. The combination of shallow water depths (<2 m) and relatively low phytoplankton Chlorophyll-a (Tokoro et al., 2014) suggests that submerged aquatic vegetation, mostly seagrass, was responsible for the majority of this CO_2 uptake. As with the remaining large-tidal sites, the strong power at the M2 period for most variables (Figure 7d) supports tidal forcing as a key driver of FCO_2 .

3.4. Air-Side Physical Drivers of FCO_2

Numerous factors contribute to the physical forcing of gas transfer in shallow coastal waters, including friction with the bottom (Rosentreter et al., 2017; Zappa et al., 2003), water-side convection (Podgrajsek et al., 2015; Van Dam, Edson, & Tobias, 2019), breaking waves, and biogenic surfactants. Nevertheless, wind speed remains the most commonly used driver in gas transfer parameterization, even in coastal waters. While a rigorous quantification of gas transfer rates is beyond the scope of this study, our data set contains valuable information on the turbulent processes responsible for air-sea gas exchange and may help to illustrate features that are globally consistent or variable. Such a comparison is currently absent from the coastal gas-transfer literature.

In the open ocean, the transfer of momentum (and therefore gas) between the sea and air is strongly associated with the wind stress (τ), which is proportional to the atmospheric friction velocity (u_*) through $\tau \sim u_*^2$ (Upstill-Goddard, 2006). The shape of the relationship between wind speed and u_* , therefore, is of great interest. When sites are mostly surrounded by water, such that the flux footprint is aquatic across most wind directions (FU, OES), u_* increases linearly with wind speed (U_z), at a slope of approximately 0.035 (Figures 8c and 8e). At the remaining sites, which experience a terrestrial influence at certain wind directions (BA, EES, AR), there is a clear dependence of the slope on wind direction (Figures 8a, 8b, and 8d). At these sites, when the wind direction is such that the flux footprint is entirely aquatic (blue points for Figures 8a and 8b), u_* scales with wind speed at the same 0.035 slope. However, when a terrestrial influence is likely (e.g., winds between 180 and 360° at BA), the slope between u_* and wind speed increases and becomes variable, as expected for relatively rough terrestrial surfaces. Since a terrestrial influence is not desirable for the present study, we discarded FCO_2 values when this ratio was greater than 150% of the average u_*/U_z (i.e., when $u_*/U_z > 1.5 * 0.0924$). The associated threshold slope of u_*/U_z (0.139) is shown as the red line in Figure 8.

The nature of momentum transfer (and thereby gas transfer) can be further assessed through the drag coefficient associated with the measurement height z ($C_{D(z)}$), which is related to the aforementioned ratio of u_*/U_z through $C_{D(z)} = \left(\frac{u_*}{U_z}\right)^2$, where U_z is the wind speed (m s^{-1}) at the measured height. At all sites, calculated values of $C_{D(z)}$ were highly variable with wind speed, but generally exceed parameterizations for the open ocean by a factor of at least 5–10 (Figure 9a). The general distribution of $C_{D(z)}$ with U_z fits the pattern observed in Vickers et al. (2013), who describe three main domains, where (1) $C_{D(z)}$ is large, and not

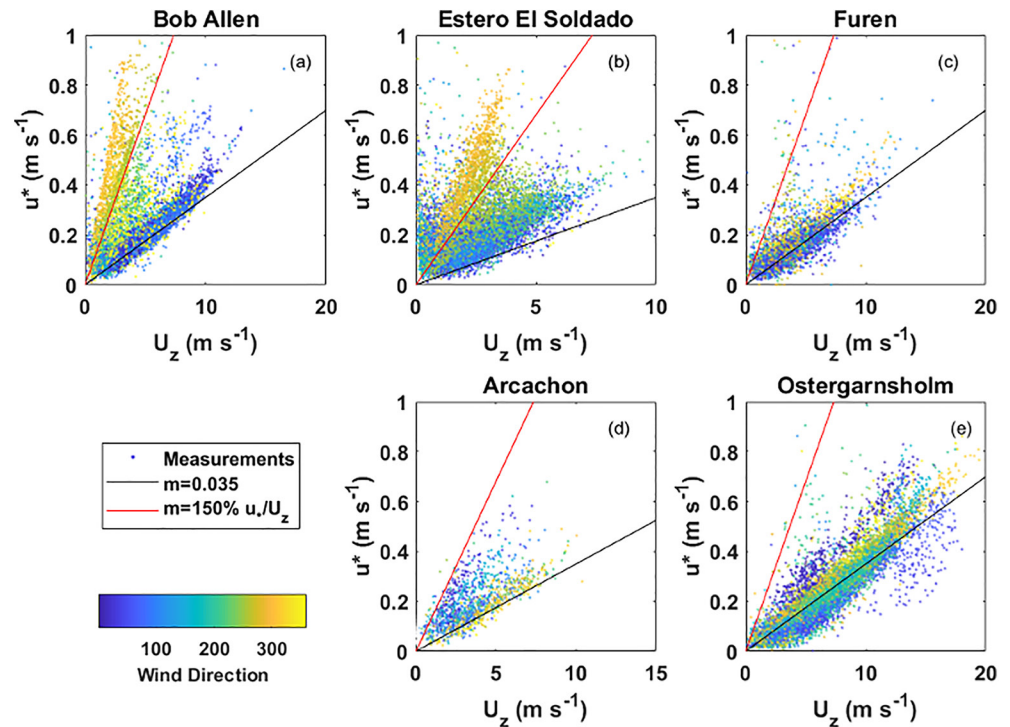


Figure 8. Wind speed at measurement height (U_z) versus friction velocity (u^*) across sites, colored by wind direction. The black line is a reference slope of 0.035, and the slope of the red line is set at 0.139, or 150% of the average u^*/U_z ratio from this study (slope = 0.139 = 1.5 × 0.924).

strongly related to U_z (1–4 m s⁻¹), (2) moderate winds (4–10 m s⁻¹) where $C_{D(z)}$ is constant at ~0.01, and (3) a regime of increasing $C_{D(z)}$ at U_z greater than 10 m s⁻¹ (only visible for BA and OES in Figures 9b and 9f).

The elevation in $C_{D(z)}$ above values expected for the open ocean may be related to the increased roughness of immature, “growing” waves under fetch-limited conditions (Mahrt et al., 1996; Rutgersson et al., 2020; Vickers & Mahrt, 1997). Small-scale non-stationary winds have been shown to enhance fluxes above the theoretical expectations for lower wind speeds in marine conditions (Mahrt et al., 2020). This $C_{D(z)}$ enhancement may be related to “disturbed” or “growing” wave fields which may be present at low, as well as high, wind speeds (Rutgersson et al., 2020). These “growing” wave fields under non-stationary conditions may offer a possible explanation for the observed increase in $C_{D(z)}$ at wind speeds between 1 and 5 m s⁻¹ (Figure 9a).

However, it is clear that other factors may also contribute to this $C_{D(z)}$ enhancement, including bottom-driven turbulence, surfactant activity, shallow water depth (more rapid wave breaking) and the presence of additional submerged roughness elements (i.e., seagrasses). For example, at very low wind speeds, the combination of increased air-side convection and unstable-to-neutral conditions has been associated with enhanced gas transfer rates (Sahlee et al., 2008; Van Dam, Lopes, et al., 2020). However, this effect is not clear in the present data set, as atmospheric stability (z/L) was not related to these periods of increased $C_{D(z)}$ (not shown).

3.5. Global Trends

While LE fluxes exhibited a significant latitudinal trend, with net evaporative heat losses increasing towards the equator (Figure 6d), such a trend was not apparent for FCO₂ (Figure 6b). Instead, tidal forcing appeared as the key global driver of FCO₂ trends in seagrass meadows, with large-tidal sites exhibiting a greater FCO₂ range (Figure 4), and magnitude toward a CO₂ sink status (Figure 6a), than small-tidal sites. Furthermore, small-tidal sites (BA, OES) responded strongly to variability at time scales longer than a day (Section 3.3.1), while the large-tidal sites (EES, FU, FK) were more sensitive to variability at the M2 and daily time scales

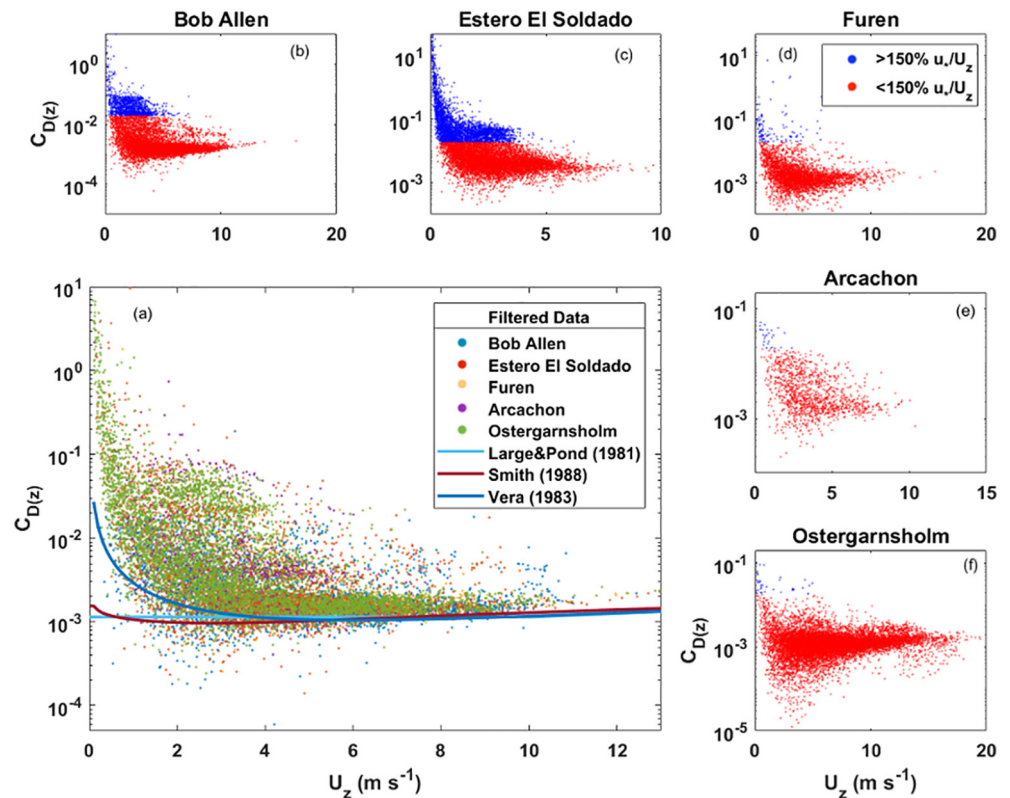


Figure 9. Relationship between U_z and $C_{D(z)}$, after filtering by the u^*/U_z threshold (a). A selection of open-ocean relationships from the literature is depicted in the solid lines. Similar scatterplots for individual sites, showing all data (b–f), including measurements where u^*/U_z exceeded the 150% threshold which are represented by the blue points.

(Section 3.3.2). Many factors may contribute to this global trend in tidal forcing of air-water CO₂ exchange. Tidal currents can enhance rates of gas transfer when bottom-generated turbulence impacts the air-water interface (Ho et al., 2014; Rosentreter et al., 2017; Upstill-Goddard, 2006), but under certain conditions may suppress gas transfer when currents are strong enough to re-suspend sediments (Abril et al., 2009). Similarly, tidal impacts on sediment biogeochemical cycling can cause variations in the air-water CO₂ gradient. Sediment resuspension and tidal oxygen pumping can enhance rates of aerobic respiration enhancing CO₂ release (Almroth-Rosell, et al., 2012; Ståhlberg et al., 2006). Elsewhere, current can generate pressure gradients which flush anaerobic respiration products from sediments, either increasing or decreasing pCO₂ in proportion to DIC and alkalinity fluxes (Santos et al., 2015). At a larger scale, tidal mixing drives inorganic carbon “outwelling” from coastal marshes (Cai et al., 1999), with an effect on air-water CO₂ exchange that should be proportional to the DIC:TA export ratio.

Because these factors act synchronously and are often correlated with each other, it is impossible to attribute the global trend of decreasing magnitude and range in FCO₂ with a single “tidal” factor. For example, tidal mixing may interact with allochthonous factors, driving net CO₂ release via DIC “outwelling” (Polse-naere et al., 2012; Volta et al., 2020), or enhancing CO₂ uptake through coastal wetland alkalinity export (Akhand et al., 2020; Cai et al., 1999; Santos et al., 2015). In these cases, blue carbon assessments should be careful to avoid “double-counting” carbon that was produced or consumed in tidally connected systems. On the other hand, in less tidal regions, measured air-water CO₂ exchanges may in fact be due to autochthonous processes like calcification or respiration of buried seagrass organic matter. As the goal of the blue carbon community is to capture the impact of seagrass meadows on net carbon storage, it is critical that these “missing” CO₂ exchanges be incorporated into blue carbon budgets. Taken together, we argue that tidal dynamics should be considered during blue carbon assessments. This will help to distinguish between seagrass meadows where air-water CO₂ exchanges either reflect real blue carbon enhancement/mitigation or are simply the result of lateral fluxes.

4. Summary and Conclusion

We produced a global synthesis of all available atmospheric EC measurements of air-water CO₂ exchange (FCO₂) over shallow, seagrass-dominated environments. At most sites, the absolute magnitude of FCO₂ was as large or larger than published “blue carbon” burial rates (CBR). Elsewhere, CO₂ fluxes in excess of organic carbon storage have been reported for Japanese seagrasses (Kuwae & Hori, 2019), but the present study demonstrates that this is a global, not regional phenomenon. At seagrass meadows functioning as net sources of CO₂ to the atmosphere (BA, OES), FCO₂ was between 44 (OES) –115 (BA)% of global average CBR (0.13 μmol m⁻² s⁻¹). Assuming minimal lateral exchange, this effectively converted BA from a net carbon sink into a net carbon source. Datasets for both BA and OES contain substantial and representative measurements during all seasons (Figure 5b), indicating that while there is substantial seasonal variability (Rutgersson et al., 2020) in FCO₂, these sites are indeed both net sources of CO₂ to the atmosphere. We suggest net ecosystem calcification at BA as a putative source of this CO₂, due to the correlation between FCO₂ and temperature, and the large CaCO₃ stocks present at this site (Howard et al., 2018). We suggest that at these and other seagrass meadows with minimal tidal forcing, future blue carbon assessments should consider air-water CO₂ exchange. Here, net CO₂ release or uptake is likely driven by autochthonous processes like anaerobic alkalinity production, calcification, or respiration of recently buried seagrass organic matter, all of which do contribute to net blue carbon sequestration. For the other sites with complete seasonal data, net CO₂ uptake was ~100% (EES) to over 800% (FU) of global average CBR. At these sites, the presence of tidal forcing brings into question if or how this CO₂ uptake should be incorporated into blue carbon budgets, as it is likely driven by allochthonous factors like lateral DIC or alkalinity exchange (Akhand et al., 2020; Volta et al., 2020).

We then identified drivers of FCO₂ that are present across the large range in seagrass ecosystems, which are responsible for generating this “disagreement” between CBR and net carbon sink/source status. First, we considered the leverage exerted on FCO₂ by the physical processes affecting rates of air-water CO₂ exchange, and found that surface roughness ($C_{D(z)}$) was always greater than expected for the open ocean, suggesting a near-universal enhancement of gas transfer in shallow, coastal waters. Next, many lines of evidence point to tidal-driven exchanges as a key driver for FCO₂ over seagrass meadows. First, we show a clear relationship between tidal range and energy balance residual, which persists across our global range in study sites. This energy balance “leakage” under tidal conditions indicates that the lateral exchange of dissolved CO₂ (and organic carbon) is a major factor contributing to the observed mismatch between FCO₂ and CBR. The negative relationship between average tidal range and FCO₂ (Figure 6a) provides further evidence that the sites acting as net CO₂ sinks may have done so in response to tidal forcing. Lastly, the results of our wavelet coherence analysis support the role of tidal forcing on FCO₂, given the increase in power at the M2 period, especially for EES, AR, and FU (Figures 9b, 9c, and 9e). As discussed above, this tidal forcing has implications for blue carbon accounting, as air-water CO₂ exchange at sites with minimal tidal exchanges likely represents the combined effects of processes like anaerobic alkalinity production, calcification, or OC respiration. These “missing” carbon fluxes complicate traditional blue carbon accounting by challenging the assumption that soil OC burial constitutes a 1:1 removal of CO₂ from the atmosphere.

In conclusion, we report high rates of air-water CO₂ exchange over seagrass meadows, which may significantly alter the net carbon storage capacity of these “blue carbon” ecosystems. This study argues the need for a more comprehensive approach to future “blue carbon” assessments, which should consider organic carbon storage in the context of other carbon fluxes, including air-water CO₂ exchange. Future studies can build on this work by investigating the role of tidal and thermal forcing, which may affect CO₂ fluxes by enhancing (or suppressing) the turbulence responsible for air-water gas exchange, but may also transport excess CO₂ away from or to seagrass meadows. And, while the present study was limited to CO₂, many of the factors affecting air-sea CO₂ transfer are also applicable to other greenhouse gases including CH₄ and N₂O. There is also a clear need for direct CO₂ flux measurements in the southern hemisphere, of which none are presently available.

Data Availability Statement

Data are published openly at <https://doi.org/10.6084/m9.figshare.12161478.v1> for BA, and 10.5281/zenodo.3372787 for EES (Barreras-Apodaca & Sánchez-Mejía, 2019). The remaining datasets for FU, FK, AR, and OES are available under previous publications Tokoro et al. (2014), Polsenaere et al. (2012), and Rutgersson et al. (2020).

Acknowledgments

This work was primarily supported by the DAAD grant #57429828, from funds of the German Federal Ministry of Education and Research (BMBF). This work was supported by the US National Science Foundation through the Florida Coastal Everglades Long-Term Ecological Research program under Grants No. DEB-1237517 and DEB-1832229. We thank Dr Mary Zeller and three anonymous reviewers as well as the associate editor for their feedback on this manuscript, which significantly improved its quality. We appreciate the assistance of the National Parks Service, who allowed equipment to be deployed in the Everglades National Park at Bob Allen Keys, under Permit [EVER-2018-SCI-0072]. Measurements at Estero El Soldado were possible with funds from the Mexican National Council of Science and Technology (CONACYT) grant #278608 and assistance from the Ecology Commission from Sonora (CEDES). This is contribution #254 from the Coastlines and Oceans Division in The Institute of Environment at Florida International University. TK and TT were funded in part by Grants-in-Aid for Scientific Research (KAKEN-HI) grant numbers JP18H04156 from the Japan Society for the Promotion of Science. The Östergarnsholm site is a part of the ICOS (Integrated Carbon Observation Study) and is funded by Swedish Research Council and Uppsala University. Technical staff working at the Östergarnsholm station are greatly acknowledged. The Arcachon study was supported by a PhD fellowship from the French Ministry of Higher Education, Research and Innovation, the ANR PROTIDAL project (2006–2009), the CNES-TOSCA SYNIHAL project (2012–2014) and the Aquitaine region; we are grateful to all our colleagues from the University of Bordeaux and INRA Bordeaux who participated to AR EC field deployments and data analysis. The authors declare no conflicts of interest. Open access funding enabled and organized by Projekt DEAL.

References

Abril, G., Commarieu, M.-V., Sottolichio, A., Bretel, P., & Guérin, F. (2009). Turbidity limits gas exchange in a large macrotidal estuary. *Estuarine, Coastal and Shelf Science*, 83(3), 342–348. <https://doi.org/10.1016/j.ecss.2009.03.006>

Akhand, A., Watanabe, K., Chanda, A., Tokoro, T., Chakraborty, K., Moki, H., et al. (2020). Lateral carbon fluxes and CO₂ evasion from a subtropical mangrove-seagrass-coral continuum. *Science of the Total Environment*, 752, 142190. <https://doi.org/10.1016/j.scitotenv.2020.142190>

Al-Haj, A. N., & Fulweiler, R. W. (2020). A synthesis of methane emissions from shallow vegetated coastal ecosystems. *Global Change Biology*, 26(5), 2988–3005. <https://doi.org/10.1111/gcb.15046>

Almroth-Rosell, E., Tengberg, A., Andersson, S., Apler, A., & Hall, P. O. J. (2012). Effects of simulated natural and massive resuspension on benthic oxygen, nutrient and dissolved inorganic carbon fluxes in Loch Creran, Scotland. *Journal of Sea Research*, 72, 38–48. <https://doi.org/10.1016/j.seares.2012.04.012>

Armitage, A. R., Frankovich, T. A., & Fourqurean, J. W. (2011). Long-term effects of adding nutrients to an oligotrophic coastal environment. *Ecosystems*, 14(3), 430–444. <https://doi.org/10.1007/s10021-011-9421-2>

Attard, K. M., Rodil, I. F., Glud, R. N., Berg, P., Norkko, J., & Norkko, A. (2019). Seasonal ecosystem metabolism across shallow benthic habitats measured by aquatic eddy covariance. *Limnology & Oceanography*, 4(3), 79–86. <https://doi.org/10.1002/lo.12107>

Aubinet, M., Grelle, A., Ibrom, A., Rannik, U., Moncrieff, J., Foken, T., et al. (2000). Estimates of the annual net carbon and water exchange of European forests: The EUROFLUX methodology. *Advances in Ecological Research*, 30, 113–175. [https://doi.org/10.1016/S0065-2504\(08\)60018-5](https://doi.org/10.1016/S0065-2504(08)60018-5)

Barreras-Apodaca, A., & Sánchez-Mejía, Z. M. (2019). *Eddy Covariance observations of three different sites from Estero El Soldado*, Sonora, Mexico. <https://doi.org/10.5281/zenodo.3372787>

Benítez-Valenzuela, L. I., & Sanchez-Mejía, Z. M. (2020). Observations of turbulent heat fluxes variability in a semiarid coastal lagoon (Gulf of California). *Atmosphere*, 11(6), 15–17. <https://doi.org/10.3390/atmos11060626>

Berg, P., Delgard, M. L., Polsenaere, P., Mcglathery, K. J., Doney, S. C., & Berger, A. C. (2019). Dynamics of benthic metabolism, O₂, and pCO₂ in a temperate seagrass meadow. *Limnology & Oceanography*, 1–19. <https://doi.org/10.1002/lno.11236>

Berg, P., Røy, H., Janssen, F., Meyer, V., Jørgensen, B., Huettel, M., & de Beer, D. (2003). Oxygen uptake by aquatic sediments measured with a novel non-invasive eddy-correlation technique. *Marine Ecology Progress Series*, 261, 75–83. <https://doi.org/10.3354/meps261075>

Borges, A. V., Vanderborcht, J.-P. P., Schiettecatie, L., Gazeau, F. F. F., Ferrón-Smith, S., Delille, B., et al. (2004). Variability of the Gas Transfer Velocity of CO₂ in a Macrotidal Estuary (the Scheldt). *Estuaries*, 0(4), 593–603. <https://doi.org/10.1007/bf02907647>

Boström, C., Baden, S. P., & Krause-Jensen, D. (2003). *The seagrasses of Scandinavia and the Baltic Sea. World Atlas of Seagrasses*. 27–37. Retrieved from <https://www.researchgate.net/publication/265032470>

Burba, G. (2010). *Eddy covariance method for scientific, industrial, agricultural, and regulatory applications*. LI-COR Biosciences (ISBN: 978-0-615-76827-4).

Burdige, D. J., Hu, X., & Zimmerman, R. C. (2010). The widespread occurrence of coupled carbonate dissolution/precipitation in surface sediments on the Bahamas Bank. *American Journal of Science*, 310(6), 492–521. <https://doi.org/10.2475/06.2010.03>

Burdige, D. J., & Zimmerman, R. C. (2002). Impact of sea grass density on carbonate dissolution in Bahamian sediments. *Limnology & Oceanography*, 47, 1751–1763. <https://doi.org/10.4319/lo.2002.47.6.1751>

Cai, W.-J., Pomeroy, L. R., Moran, M. A., & Wang, Y. (1999). Oxygen and carbon dioxide mass balance for the estuarine-intertidal marsh complex of five rivers in the Southeastern U.S. *Limnology & Oceanography*, 44(3), 639–649. <https://doi.org/10.4319/lo.1999.44.3.0639>

Carmen, B., Krause-Jensen, D., Alcoverro, T., Marbà, N., Duarte, C. M., van Katwijk, M. M., et al. (2019). Recent trend reversal for declining European seagrass meadows. *Nature Communications*, 10, 3356. <https://doi.org/10.1038/s41467-019-11340-4>

Chien, H., Zhong, Y. Z., Yang, K. H., & Cheng, H. Y. (2018). Diurnal variability of CO₂ flux at coastal zone of Taiwan based on eddy covariance observation. *Continental Shelf Research*, 162, 27–38. <https://doi.org/10.1016/j.csr.2018.04.006>

Dollar, S., Smith, S., Vink, S., Obrebski, S., & Hollibaugh, J. (1991). Annual cycle of benthic nutrient fluxes in Tomales Bay, California, and contribution of the benthos to total ecosystem metabolism. *Marine Ecology Progress Series*, 79(1–2), 115–125. <https://doi.org/10.3354/meps079115>

Duarte, C. M., Marbà, N., Gacia, E., Fourqurean, J. W., Beggins, J., Barrón, C., & Apostolaki, E. T. (2010). Seagrass community metabolism: Assessing the carbon sink capacity of seagrass meadows. *Global Biogeochemical Cycles*, 24(4), 1–8. <https://doi.org/10.1029/2010gb003793>

Duarte, C. M., Middelburg, J. J., & Caraco, N. (2005). Major role of marine vegetation on the oceanic carbon cycle. *Biogeosciences*, 2, 1–8. <https://doi.org/10.5194/bg-2-1-2005>

Dürr, H. H., Laruelle, G. G., van Kempen, C. M., Slomp, C. P., Meybeck, M., & Middelkoop, H. (2011). Worldwide typology of nearshore coastal systems: Defining the estuarine filter of river inputs to the oceans. *Estuaries and Coasts*, 34(3), 441–458. <https://doi.org/10.1007/s12237-011-9381-y>

Eyre, B., & Ferguson, A. (2002). Comparison of carbon production and decomposition, benthic nutrient fluxes and denitrification in seagrass, phytoplankton, benthic microalgae- and macroalgae-dominated warm-temperate Australian lagoons. *Marine Ecology Progress Series*, 229, 43–59. <https://doi.org/10.3354/meps229043>

Fennel, K., Alin, S., Barbero, L., Evans, W., Bourgeois, T., Cooley, S., et al. (2019). Carbon cycling in the North American coastal ocean: A synthesis. *Biogeosciences*, 16, 1281–1304. <https://doi.org/10.5194/bg-16-1281-2019>

Fourqurean, J. W., Duarte, C. M., Kennedy, H., Marbà, N., Holmer, M., Mateo, M. A., et al. (2012). Seagrass ecosystems as a globally significant carbon stock. *Nature Geosci*, 5(7), 505–509. <https://doi.org/10.1038/ngeo1477>

Friedlingstein, P., Jones, M. W., O’Sullivan, M., Andrew, R. M., Hauck, J., Peters, G. P., et al. (2019). Global carbon budget 2019. *Earth System Science Data*, 11(4), 1783–1838. <https://doi.org/10.5194/essd-11-1783-2019>

- Gazeau, F., Borges, A., Barrón, C., Duarte, C., Iversen, N., Middelburg, J., et al. (2005). Net ecosystem metabolism in a micro-tidal estuary (Randers Fjord, Denmark): Evaluation of methods. *Marine Ecology Progress Series*, 301, 23–41. <https://doi.org/10.3354/meps301023>
- Grinsted, A., Moore, J. C., & Jevrejeva, S. (2004). Application of the cross wavelet transform and wavelet coherence to geophysical time series. *Nonlinear Processes in Geophysics*, 11, 561–566. <https://doi.org/10.5194/npg-11-561-2004>
- Gutiérrez-Loza, L., Wallin, M. B., Sahlée, E., Nilsson, E., Bange, H. W., Kock, A., & Rutgersson, A. (2019). Measurement of air-sea methane fluxes in the baltic sea using the eddy covariance method. *Frontiers of Earth Science*, 7, 1–13. <https://doi.org/10.3389/feart.2019.00093>
- HELCOM. (2009). Eutrophication in the Baltic Sea – An integrated thematic assessment of the effects of nutrient enrichment and eutrophication in the Baltic Sea region. No. 115B. In *Baltic sea environment proceedings* (p. 148), Helsinki Commission. Retrieved from http://meeting.helcom.fi/c/document_library/get_file?p_l_id=79889&folderId=377779&name=DLFE-36818.pdf
- Ho, D. T., Ferrón, S., Engel, V. C., Larsen, L. G., & Barr, J. G. (2014). Air-water gas exchange and CO₂ flux in a mangrove-dominated estuary. *Geophysical Research Letters*, 41(1), 108–113. <https://doi.org/10.1002/2013gl058785>
- Honkanen, M., Tuovinen, J., Laurila, T., Mäkelä, T., Hatakka, J., & Kielosto, S. (2018). Measuring turbulent CO₂ fluxes with a closed-path gas analyzer in a marine environment. *Atmospheric Measurement Techniques*, 11, 5335–5350. <https://doi.org/10.5194/amt-11-5335-2018>
- Howard, J. L., Creed, J. C., Aguiar, M. V. P., & Fourqurean, J. W. (2018). CO₂ released by carbonate sediment production in some coastal areas may offset the benefits of seagrass “Blue Carbon” storage. *Limnology & Oceanography*, 63(1), 160–172. <https://doi.org/10.1002/lno.10621>
- Hu, X., & Burdige, D. J. (2007). Enriched stable carbon isotopes in the pore waters of carbonate sediments dominated by seagrasses: Evidence for coupled carbonate dissolution and reprecipitation. *Geochimica et Cosmochimica Acta*, 71(1), 129–144. <https://doi.org/10.1016/j.gca.2006.08.043>
- Ikawa, H., & Oechel, W. C. (2015). Temporal variations in air-sea CO₂ exchange near large kelp beds near San Diego, California. *Journal of Geophysical Research: Oceans*, 120(1), 50–63. <https://doi.org/10.1002/2014JC010229>
- Kennedy, H., Beggs, J., Duarte, C. M., Fourqurean, J. W., Holmer, M., Marbà, N., & Middelburg, J. J. (2010). Seagrass sediments as a global carbon sink: Isotopic constraints. *Global Biogeochemical Cycles*, 24(4), 1–8. <https://doi.org/10.1029/2010gb003848>
- Kuwaie, T., & Hori, M. (2019). *Blue carbon in shallow coastal ecosystems*. <https://doi.org/10.1007/978-981-13-1295-3>
- Laruelle, G. G., Cai, W. J., Hu, X., Gruber, N., Mackenzie, F. T., & Regnier, P. (2018). Continental shelves as a variable but increasing global sink for atmospheric carbon dioxide. *Nature Communications*, 9(1), 1–11. <https://doi.org/10.1038/s41467-017-02738-z>
- Legge, O., Johnson, M., Hicks, N., Jickells, T., Diesing, M., Aldridge, J., et al. (2020). Carbon on the northwest European shelf: Contemporary budget and future influences. *Frontiers in Marine Science Specialty*, 7(March). <https://doi.org/10.3389/fmars.2020.00143>
- Lluch-Cota, S.-E. (2000). Coastal upwelling in the eastern Gulf of California. *Oceanologica Acta*, 23, 731–740. [https://doi.org/10.1016/S0399-1784\(00\)00121-3](https://doi.org/10.1016/S0399-1784(00)00121-3)
- Long, M., Berg, P., & Falter, J. (2015). Seagrass metabolism across a productivity gradient using the eddy covariance, Eulerian control volume, and biomass addition techniques. *Journal of Geophysical Research: Oceans*, 120, 2676–2700. <https://doi.org/10.1002/2014JC010441>
- Macreadie, P. I., Anton, A., Raven, J. A., Beaumont, N., Connolly, R. M., Friess, D. A., et al. (2019). The future of Blue Carbon science. *Nature Communications*, 1–13. <https://doi.org/10.1038/s41467-019-11693-w>
- Macreadie, P. I., Serrano, O., Maher, D. T., Duarte, C. M., & Beardall, J. (2017). Addressing calcium carbonate cycling in blue carbon accounting. *Limnology and Oceanography Letters*, 195–201. Tyrrell 2008. <https://doi.org/10.1002/lol2.10052>
- Mahrt, L., Nilsson, E., Pettersson, H., & Rutgersson, A. (2020). Sea-surface stress driven by small-scale non-stationary winds. *Boundary Layer Meteorology*, 176, 13–33. <https://doi.org/10.1007/s10546-020-00518-9>
- Mahrt, L., Vickers, D., Howell, J., Højstrup, J., Wilczak, J. M., Edson, J., & Hare, J. (1996). Sea surface drag coefficients in the Risø air sea experiment. *Journal of Geophysical Research*, 101(C6), 14327–14335. <https://doi.org/10.1029/96JC00748>
- Mauder, M., & Foken, T. (2004). *Documentation and instruction manual of the Eddy Covariance Software Package TK2*. Bayreuth: University of Bayreuth.
- Oreska, M. P. J., McGlathery, K. J., Aoki, L. R., Berger, A. C., Berg, P., & Mullins, L. (2020). The greenhouse gas offset potential from seagrass restoration. *Scientific Reports*, 10(1), 1–15. <https://doi.org/10.1038/s41598-020-64094-1>
- Perez, D. I., Phinn, S. R., Roelfsema, C. M., Shaw, E., Johnston, L., & Iguel, J. (2018). Primary production and calcification rates of algae-dominated reef flat and seagrass communities. *Journal of Geophysical Research: Biogeosciences*, 123(8), 2362–2375. <https://doi.org/10.1029/2017JG004241>
- Plus, M., Dalloyau, S., Trut, G., Auby, I., De Montaudouin, X., Emery, É., et al. (2010). Long-term evolution (1988–2008) of *Zostera* spp. meadows in Arcachon Bay (Bay of Biscay). *Estuarine Coastal and Shelf Science*, 87(2), 357–366. <https://doi.org/10.1016/j.ecss.2010.01.016>
- Podgrajsek, S., & Rutgersson (2015). Diel cycle of lake-air CO₂ flux from a shallow lake and the impact of waterside convection on the transfer velocity. *Journal of Geophysical Research: Biogeosciences*, 120(1), 29–38. <https://doi.org/10.1002/2014JG002781>
- Polsenaere, P., Lamaud, E., Lafon, V., Loustau, D., Delille, B., Deborde, J., et al. (2012). Spatial and temporal CO₂ exchanges measured by Eddy Covariance over a temperate intertidal flat and their relationships to net ecosystem production. *Biogeosciences*, 9(1), 249–268. <https://doi.org/10.5194/bg-9-249-2012>
- Prentice, C., Poppe, K. L., Lutz, M., Murray, E., Stephens, T. A., Spooner, A., et al. (2020). A synthesis of blue carbon stocks, sources, and accumulation rates in Eelgrass (*Zostera marina*) Meadows in the Northeast Pacific. *Global Biogeochemical Cycles*, 34(2), 1–16. <https://doi.org/10.1029/2019gb006345>
- Rey-sánchez, A. C., Bohrer, G., Morin, T. H., Shlomo, D., & Mirfenderesgi, G. (2017). Evaporation and CO₂ fluxes in a coastal reef: An eddy covariance approach. *Ecosystem Health and Sustainability*, 3(10). <https://doi.org/10.1080/20964129.2017.1392830>
- Röhr, M. E., Holmer, M., Baum, J. K., Björk, M., Chin, D., Chalifour, L., et al. (2018). Blue carbon storage capacity of Temperate Eelgrass (*Zostera marina*) Meadows. *Global Biochemical Cycles*, 1457–1475. <https://doi.org/10.1029/2018GB005941>
- Rosentreter, J. A., Maher, D. T., Ho, D. T., Call, M., Barr, J. G., & Eyre, B. D. (2017). Spatial and temporal variability of CO₂ and CH₄ gas transfer velocities and quantification of the CH₄ microbubble flux in mangrove dominated estuaries. *Limnology & Oceanography*, 62(2), 562–578. <https://doi.org/10.1002/lno.10444>
- Rutgersson, A., Pettersson, H., Nilsson, E., Bergström, H., Marcus, B. E., Wallin, E., et al. (2020). Using land-based stations for air-sea interaction studies. *Tellus A: Dynamic Meteorology and Oceanography*, 72(1), 1–23. <https://doi.org/10.1080/16000870.2019.1697601>
- Saderne, V., Gerald, N. R., Macreadie, P. I., Maher, D. T., Middelburg, J. J., Serrano, O., et al. (2019). Role of carbonate burial in Blue Carbon budgets. *Nature Communications*, 10. <https://doi.org/10.1038/s41467-019-08842-6>
- Sahlée, E., Smedman, A.-S., Högström, U., & Rutgersson, A. (2008). Reevaluation of the bulk exchange coefficient for humidity at sea during unstable and neutral conditions. *Journal of Physical Oceanography*, 38(1), 257–272. <https://doi.org/10.1175/2007jpo3754.1>

- Samper-Villarreal, J., Mumby, P. J., Saunders, M. I., Barry, L. A., Zawadzki, A., Heijnis, H., et al. (2018). Vertical accretion and carbon burial rates in subtropical seagrass meadows increased following anthropogenic pressure from European colonisation. *Estuarine, Coastal and Shelf Science*, 202, 40–53. <https://doi.org/10.1016/j.ecss.2017.12.006>
- Sanders, C. J., Maher, D. T., Smoak, J. M., & Eyre, B. D. (2019). Large variability in organic carbon and CaCO₃ burial in seagrass meadows: A case study from three Australian estuaries. *Marine Ecology Progress Series*, 616, 211–218. <https://doi.org/10.3354/meps12955>
- Santos, I. R., Beck, M., Brumsack, H.-J. J., Maher, D. T., Dittmar, T., Waska, H., & Schnetger, B. (2015). Porewater exchange as a driver of carbon dynamics across a terrestrial-marine transect: Insights from coupled 222Rn and pCO₂ observations in the German Wadden Sea. *Marine Chemistry*, 171, 10–20. <https://doi.org/10.1016/j.marchem.2015.02.005>
- Ståhlberg, C., Bastviken, D., Svensson, B. H., & Rahm, L. (2006). Mineralisation of organic matter in coastal sediments at different frequency and duration of resuspension. *Estuarine, Coastal and Shelf Science*, 70(1–2), 317–325. <https://doi.org/10.1016/j.ecss.2006.06.022>
- Takahashi, T., Sutherland, S. C., Sweeney, C., Poisson, A., Metz, N., Tilbrook, B., et al. (2002). Global sea – air CO₂ flux based on climatological surface ocean pCO₂, and seasonal biological and temperature effects. *Deep Sea Research Part II: Topical Studies in Oceanography*, 49(9–10), 1601–1622. [https://doi.org/10.1016/S0967-0645\(02\)00003-6](https://doi.org/10.1016/S0967-0645(02)00003-6)
- Tokoro, T., Hosokawa, S., Miyoshi, E., Tada, K., Watanabe, K., Montani, S., et al. (2014). Net uptake of atmospheric CO₂ by coastal submerged aquatic vegetation. *Global Change Biology*, 20(6), 1873–1884. <https://doi.org/10.1111/gcb.12543>
- Torrence, C., & Compo, G. P. (1998). A practical guide to wavelet analysis. *Bulletin of the American Meteorological Society*, 79, 61–78. [https://doi.org/10.1175/1520-0477\(1998\)079<0061:APGTWA>2.0.CO;2](https://doi.org/10.1175/1520-0477(1998)079<0061:APGTWA>2.0.CO;2)
- Upstill-Goddard, R. C. (2006). Air–sea gas exchange in the coastal zone. *Estuarine, Coastal and Shelf Science*, 70(3), 388–404. <https://doi.org/10.1016/j.ecss.2006.05.043>
- Van Dam, B. R., Edson, J. B., & Tobias, C. (2019). Parameterizing air-water gas exchange in the shallow, microtidal new river estuary. *Journal of Geophysical Research: Biogeosciences*, 124, 2351–2363. <https://doi.org/10.1029/2018JG004908>
- Van Dam, B. R., Lopes, C., Osburn, C. L., & Fourqurean, J. W. (2019). Net heterotrophy and carbonate dissolution in two subtropical seagrass meadows. *Biogeosciences*, 16, 4411–4428. <https://doi.org/10.5194/bg-2019-191>
- Van Dam, B. R., Lopes, C. C., Polsenaere, P., Price, R. M., Rutgersson, A., & Fourqurean, J. W. (2020). Water temperature control on CO₂ flux and evaporation over a subtropical seagrass meadow revealed by atmospheric eddy covariance. *Limnology & Oceanography*, 66, 1–18. <https://doi.org/10.1002/lno.11620>
- Vickers, D., & Mahrt, L. (1997). Fetch limited drag coefficients. *Boundary-Layer Meteorology*, 85, 53–79. <https://doi.org/10.1023/A:1000472623187>
- Vickers, D., Mahrt, L., & Andreas, E. L. (2013). Estimates of the 10-m Neutral Sea Surface Drag Coefficient from Aircraft Eddy-Covariance Measurements. *Journal of Physical Oceanography*, 43(2), 301–310. <https://doi.org/10.1175/JPO-D-12-0101.1>
- Volta, C., Ho, D. T., Maher, D. T., Wanninkhof, R., Friederich, G., Del Castillo, C., & Dulai, H. (2020). Seasonal variations in dissolved carbon inventory and fluxes in a mangrove-dominated estuary. *Global Biogeochemical Cycles*, 34, e2019GB006515. <https://doi.org/10.1029/2019GB006515>
- Wanninkhof, R., Asher, W. E., Ho, D. T., Sweeney, C., & McGillis, W. R. (2009). Advances in quantifying air-sea gas exchange and environmental forcing. *Annual Review of Marine Science*, 1(1), 213–244. <https://doi.org/10.1146/annurev.marine.010908.163742>
- Zappa, C. J., Raymond, P. A., Terray, E. A., & McGillis, W. R. (2003). Variation in surface turbulence and the gas transfer velocity in a macro-tidal estuary. *Estuaries*, 26(6), 1401–1415. <https://doi.org/10.1007/BF02803649>